UNIVERSITÄT AUGSBURG
Universitätsbibliothek

OPEN ACCESS
OPUS AUGSBURG

Non-linear dependence of ion heat flux on plasma density at the L–H transition of JET NBI-heated deuterium–tritium plasmas

P. Vincenzi, E. R. Solano, E. Delabie, C. Angioni, Gregor Birkenmeier, C. Maggi, R. B. Morales, H. J. Sun, E. Tholerus

Angaben zur Veröffentlichung / Publication details:

Vincenzi, P., E. R. Solano, E. Delabie, C. Angioni, Gregor Birkenmeier, C. Maggi, R. B. Morales, H. J. Sun, and E. Tholerus. 2025. "Non-linear dependence of ion heat flux on plasma density at the L–H transition of JET NBI-heated deuterium–tritium plasmas." *Nuclear Fusion* 64 (1): 016038. https://doi.org/10.1088/1741-4326/ad96cd.

Nutzungsbedingungen / Terms of use: **CC BY 4.0**

Dieses Dokument wird unter folgenden Bedingungen zur Verfügung gestellt: / This document is made available under these conditions:
CC-BY 4.0: Creative Commons: Namensnennung
Weitere Informationen finden Sie unter: / For more information see:
https://creativecommons.org/licenses/by/4.0/deed.de

nuclear fusion
IAEA

PAPER • OPEN ACCESS

Non-linear dependence of ion heat flux on plasma density at the L–H transition of JET NBI-heated deuterium–tritium plasmas

To cite this article: P. Vincenzi *et al* 2025 *Nucl. Fusion* **65** 016038

View the article online for updates and enhancements.

You may also like

- Power balance analysis at the L-H transition in JET-ILW NBI-heated deuterium plasmas
P Vincenzi, E R Solano, E Delabie et al.
- Recent progress in L–H transition studies at JET: tritium, helium, hydrogen and deuterium
E.R. Solano, E. Delabie, G. Birkenmeier et al.
- L-H transition physics in hydrogen and deuterium: key role of the edge radial electric field and ion heat flux
F Ryter, M Cavedon, T Happel et al.

This content was downloaded from IP address 137.250.102.76 on 16/10/2026 at 09:15

OPEN ACCESS
IOP Publishing | International Atomic Energy Agency
Nuclear Fusion
Nucl. Fusion **65** (2025) 016038 (12pp)
https://doi.org/10.1088/1741-4326/ad96cd

Non-linear dependence of ion heat flux on plasma density at the L–H transition of JET NBI-heated deuterium–tritium plasmas

P. Vincenzi[1,2,*], E.R. Solano[3], E. Delabie[4], C. Angioni[5], G. Birkenmeier[5,6], C. Maggi[7], R.B. Morales[7], H.J. Sun[7], E. Tholerus[7] and JET Contributors[a]

[1] Consorzio RFX (CNR, ENEA, INFN, Universit̀a di Padova, Acciaierie Venete SpA), Corso Stati Uniti 4, 35127 Padova, Italy
[2] Institute for Plasma Science and Technology, CNR, Padova, Italy
[3] Laboratorio Nacional de Fusión, CIEMAT, Madrid, Spain
[4] Oak Ridge National Laboratory, Oak Ridge, TN 37831, United States of America
[5] Max-Planck-Institut für Plasmaphysik, D-85748 Garching, Germany
[6] TUM School of Natural Sciences, Physics Department, Technical University of Munich, 85748 Garching, Germany
[7] UKAEA (United Kingdom Atomic Energy Authority), Culham Campus, Abingdon, Oxfordshire OX14 3DB, United Kingdom of Great Britain and Northern Ireland

E-mail: pietro.vincenzi@igi.cnr.it

Received 20 August 2024, revised 4 November 2024
Accepted for publication 25 November 2024
Published 5 December 2024



Abstract

Recent JET D–T campaigns opened the possibility of unique isotope studies to investigate the L–H transition physics in view of reactor plasmas and to study the origin of the observed power threshold minimum. In the present paper, we characterise L–H transitions in the low and high-density branches of JET NBI-heated D–T plasmas. As discussed in the paper, L–H transition has been hypothesised to be determined by the transport power losses of plasma ions, i.e. the so-called ion heat flux (Q_i). We present the first power balance analysis of JET NBI-heated D–T plasmas to evaluate the ion heat flux at the transition. Due to the experimental setting being similar to previous JET D experiments, we also directly compare the results, discussing the isotope effect and similarities between datasets. First, we find an isotope effect between D and D–T Q_i, with a lower Q_i in D–T plasmas. We confirm that the ion heat flux deviates from density linearity compared to the linear trend observed in wave-heated D plasmas of other tokamaks. The deviation we observe in NBI-heated L–H transitions happens at an isotope-dependent density. Plasma edge rotation correlates with Q_i deviation from density linearity in the low-density branch. However, further investigations would be required to assess the role of rotation on Q_i and the power threshold minimum at JET. At low plasma density, NBI

[a] See Maggi *et al* 2024 (https://doi.org/10.1088/1741-4326/ad3e16) for JET Contributors.
[*] Author to whom any correspondence should be addressed.

Original content from this work may be used under the terms of the Creative Commons Attribution 4.0 licence. Any further distribution of this work must maintain attribution to the author(s) and the title of the work, journal citation and DOI.

 © 2024 The Author(s). Published by IOP Publishing Ltd on behalf of the IAEA

power dominates Q_i, while increasing the density makes the equipartition power dominant. We finally compare our results with hypotheses proposed from evidence in other tokamaks to present a complete overview of ion heat flux analyses in D and D–T NBI-heated plasmas at JET.

Keywords: L–H transition, H-mode, ion heat flux, JET, deuterium–tritium, isotope effect

(Some figures may appear in colour only in the online journal)

1. Introduction

The high confinement mode is a transport regime with enhanced particle and energy confinement that will be exploited in ITER [1] to achieve its main objectives. The transition from low confinement (L-mode) to high confinement (H-mode) transport regime happens when a certain power threshold ($P_{L–H}$) is exceeded by the net power loss through the plasma surface (P_{loss}). P_{loss} is defined as:

$$\boldsymbol{P_{loss} = P_{aux} + P_{\alpha} + P_{ohm} - \frac{dW}{dt}} \quad (1)$$

where P_{aux} is the auxiliary heating power, P_{α} is the fusion power carried by alphas (if any), P_{ohm} is the ohmic power, dW/dt is the temporal changes of the plasma energy content W, taken into account due to the power ramp that drives the plasma towards the transition. When discussing L–H transitions, we sometimes refer to the non-radiating power flowing through the separatrix (P_{sep}), being $P_{sep} = P_{loss} - P_{rad}$ (P_{rad} is the radiated power inside the last closed flux surface (LCFS)).

A comprehensive L–H power threshold scaling law, obtained from a multi-machine database of Deuterium plasmas is the so-called 'ITPA 2008' scaling law [2], which yields:

$$\boldsymbol{P_{L-H}\,[MW] = 0.049\overline{n_e}^{0.72} B_T^{0.8} S^{0.94}} \quad (2)$$

with the line averaged electron density $\overline{n_e}$ in 10^{20} m^{-3}, the toroidal magnetic field B_T in T, and the plasma surface S in m^2.

$P_{L–H}$ scaling laws and understanding the L–H transition are crucial for ITER operation and DEMO design since they affect the prediction of plasma performance and reactor size [3].

Among other parameters that are known to influence the L–H transition (see e.g [4].), plasma isotope mass has been shown to have an impact on $P_{L–H}$, for instance, during the first JET D–T experimental campaign in 1997 [5]. It was concluded that, for hydrogenic species, the power threshold scales as $P_{L–H} \propto A_{eff}^{-1}$, A_{eff} being the effective plasma isotope mass. $P_{L–H}$ in equation (2) can be extended to other hydrogenic plasmas with the factor $\frac{2}{A_{eff}}$, although $P_{L–H}$ is observed to vary significantly even with the same A_{eff} [6].

ITPA 2008 scaling law (equation (2)) has been derived mainly from C-wall devices. JET [7] and ASDEX-Upgrade (AUG) [8] reported a reduction of the L–H power threshold of ∼30% by installing a full metal wall. A new JET-specific scaling law has been derived only from JET metal wall L–H transitions [9, 10] within the ITPA task TC-26. The 'TC26' JET scaling law strongly depends on the divertor configuration. We report here the scaling for the JET horizontal target configuration that is of interest for this publication:

$$\boldsymbol{P_{L-H,TC26,JET} = 0.057\bar{n}_e^{1.43} B_t^{0.77} S^1} \quad (3)$$

where we note a larger exponent on plasma density with respect to equation (2), suggesting that, in JET, the $P_{L–H}$ reduction with the metal wall is seen at densities below $\sim 10^{20}$ m^{-3}.

$P_{L–H}$ scaling laws are valid in the so-called high-density branch of the L–H transition, i.e. when $P_{L–H}$ increases monotonically with plasma density. Often, $P_{L–H}$ shows a minimum at a corresponding density called minimum density, $n_{e,min}$. Below this power minimum, in some cases, $P_{L–H}$ is seen to increase again when plasma density is decreased (in the so-called 'low-density branch'). This behaviour was first reported in COMPASS tokamak [11], characterised then in other tokamaks (e.g. [12–14]) and observed for some divertor geometries also at JET with the C-wall [15–17]. At JET, $n_{e,min}$ reappeared with the installation of the full metal wall. The minimum density $n_{e,min}$, when observed, is seen to depend on the magnetic field, plasma shape and current [7, 15, 18, 19]. At JET, $n_{e,min}$ is shown to be affected by a strong isotope effect, being lower for higher effective mass [4, 10, 20].

Equation (1) can be written as the sum of the power carried by plasma ions, Q_i, and the power carried by electrons, Q_e: $P_{loss} = Q_i + Q_e$. In particular:

$$\boldsymbol{Q_i = P_{aux,i} + P_{\alpha,i} + P_{ei} - dW_i/dt} \quad (4)$$

$$\boldsymbol{Q_e = P_{aux,e} + P_{\alpha,e} + P_{ohm} - P_{ei} - dW_e/dt} \quad (5)$$

where we introduced the ion–electron power exchange term P_{ei} (often called 'equipartition power') and the energy of plasma ions W_i. P_{ei} is proportional to the volume integral of $n_e n_i (T_e - T_i)/T_e^{3/2}$, and it is positive for $T_e > T_i$. Q_i is also called 'ion heat flux' or 'ion heat flow'. Subscripts 'i' and 'e' identify the power terms coupled to plasma ions and electrons, respectively.

In wave-heated Deuterium plasmas in AUG and Alcator C-mod (C-mod) tokamaks, the L–H power threshold is observed to have a non-monotonic dependency on density as in many other devices, while the power coupled to ions Q_i is seen to keep linearly increasing with density, throughout both density branches [8, 19, 21–23]. It has been proposed that a critical edge ion heat flux is necessary to trigger the L–H transition and that the L–H power threshold non-monotonic density dependence is explained by the equipartition power between

electrons and ions, which strongly decreases the power flowing to plasma ions at low density. Indeed, with dominant electron heating, the auxiliary wave-heating power coupled to the plasma must be increased to generate a larger difference in electron-to-ion temperature that compensates for the P_{ei} decrease at low density. A different behaviour has been noted for deuterium Neutral Beam Injection (NBI)-heated L–H transitions, both at AUG [19] and JET [24], with the ion heat flux departing from linearity in density in the low-density branch. In NBI-heated plasmas, the ion heat flux criterion for the H-mode access may, therefore, not apply, at least below $n_{e,min}$. It is clear that $n_{e,min}$ prediction and H-mode access criterion have strong implications for H-mode scenarios in future reactor-like experiments such as ITER.

At JET, a complete hydrogenic isotope scan has been recently completed, including D–T plasmas [25], with dedicated experiments on L–H transition [4, 10]. In the present paper, we aim at characterising the L–H transitions at different densities of NBI-heated deuterium–tritium plasmas. We present the first (and possibly last, before ITER) power balance analysis at the L–H transition of D–T NBI-heated plasmas. The scope of this paper is then to evaluate the role of the different terms contributing to P_{loss} just before H-mode access, especially characterising the ion heat flux at different D–T plasma densities. Experimental settings used for D–T plasmas correspond to what was used for the JET NBI-heated deuterium dataset analysed in [24], allowing a direct comparison between the present D–T dataset and its D counterpart. We compare D–T with previous D results to discuss the isotope effect on the ion heat flux. Experimental settings, measurement processing procedure, and power balance analysis methodology are similar to previous D dataset analysis [24], to which we refer for details not repeated in this paper.

The paper is organised as follows: we first present the experimental dataset in section 2, where we also characterise L–H transitions. In section 3, we describe the power balance analysis of the D–T dataset, presenting the ion heat flux analysis results. In section 4, we investigate the origin of Q_i in JET NBI-heated L–H transitions, we compare D and D–T plasmas, and we discuss their Q_i deviation from density linearity seen in wave-heated plasmas of AUG and C-mod tokamaks. We conclude the paper by summarising the main results in section 5.

2. Experimental database description and L–H transition characterisation

The dataset considered for this work consists of seven L–H transitions in JET deuterium–tritium plasmas heated by NBI, where L-mode plasma density in five different shots has been controlled to vary from low to high-density branches. Other parameters that are known to influence P_{L-H} have been kept constant among shots, such as the toroidal magnetic field, set to 3 T, and the plasma current, 2.5 MA, at the same single-null 'horizontal target' (HT) divertor configuration, where the outer strike point is on an almost horizontal divertor tile and the inner one on a vertical tile. As for usual operations at JET, the $\overrightarrow{\boldsymbol{B}} \times \nabla \mathbf{B}$ drift has been directed downwards toward the X-point. Plasma effective charge Z_{eff}, measured by the Bremsstrahlung diagnostic [26], is within 1.2 and 1.5. The D–T isotope concentration, measured by high-resolution hydrogenic Balmer α-light spectroscopy [27] and Optical Penning Gauge technique [28], has been kept close to 50:50, except for some L–H transitions, e.g. in shot 99 470 and 99 471, which are Tritium-rich (see table 1). Unbalances in D–T concentration, though unavoidable, are not a significant concern for our L–H power balance analysis, since, for plasma mixtures, P_{L-H} is not seen to vary linearly with $1/A_{eff}$ for isotope mixtures [6]. Traces of hydrogen are present ($<2\%$) and are not considered in the transport simulations for the power balance analysis (see section 3). Auxiliary power from deuterium-only or deuterium–tritium NBI (where D injection is from octant 4 and T from oct. 8) [29] has been used to trigger the L–H transition. Auxiliary power is slowly increased ($\sim$1 MW s^{-1}, in steps of 1 MW) to identify the L–H transition time and power threshold clearly. A summary of the L–H transitions considered for this paper is reported in table 1, listing plasma isotope concentration, plasma density, and NBI-related quantities (evaluated by ASCOT code [30]) at the time considered for the L–H transition analysis. For pulses 104 511 and 99 472, we considered two different transitions generated by two separate NBI power ramps.

L–H transitions are commonly identified by a simultaneous increase of the edge density and/or temperature and a drop of the hydrogenic Balmer α-light emission in the divertor region, with the plasma then permanently staying in H-mode. For this study, the analysis is done at the last L-mode time before the transition when kinetic plasma measurements are available. Since dithers often affect the L–H transition, especially at high density, and they can perturb the interpretation of profile measurements, when present, we decided to exclude them and anticipate the analysis time. This choice, similar to what was done in a previous power balance study [24], has a negligible effect on P_{loss}, which does not vary significantly during the dithering phases. Therefore, the dithering phase does not impact the observed P_{L-H} trend in density. However, it slightly affects the transition density, which slowly rises during dithers, even with constant fuelling and power. Figure 1 shows relevant time traces for the L–H transition identification in our dataset and reports both the identified L–H transition time defined for JET and the chosen analysis time, constrained as discussed. In the low-density branch, we often see transitions to M-mode [31] (e.g. in 104 511 and 99472_1st), while transitions 99 470 and 99472_2nd display dithers before the transition, typical of the high-density branch side of the $n_{e,min}$ region. Increasing density, divertor oscillations, and brief dithers, appear (99471 and 99472_2nd).

P_{loss} at the L–H transition is plotted versus the line-averaged density in figure 2, also including other transitions that are not explicitly analysed in this work but that can be useful to characterise L–H transition density branches. D–T (isotope-corrected) ITPA 2008 (equation (2))

Table 1. Summary of the NBI-heated, D–T plasma dataset considered for the L–H transition analysis. Quantities are evaluated at the L–H transition analysis time.

shot	D:T concentration % (A_{eff})	Density branch	Line-averaged electron density (10^{19} m^{-3})	NBI species	NBI power coupled to plasma (MW)	NBI power coupled to ions	NBI power coupled to electrons	NBI injected torque (Nm)
104 511 (1st transition)	51:49 [2.50]	Low	2.4	D	3.2	59.6%	40.4%	5.1
104 511 (2nd transition)	53:47 [2.50]	Low	2.8	D	4.2	58.5%	41.5%	6.8
99 472 (1st transition)	43:57 [2.55]	Low/Near-minimum	2.9	D and T	3.1	58.1%	41.9%	4.8
99 470	28:72 [2.70]	Minimum	3.0	D and T	2.0	44.8%	55.2%	3.3
99 472 (2nd transition)	42:58 [2.56]	High/Near-minimum	3.1	D and T	1.2	45.9%	54.1%	3.6
99 471	39:61 [2.59]	High	3.8	D and T	3.0	48.9%	51.1%	4.6
99 474 (2nd transition)	41:59 [2.58]	High	4.4	D and T	3.9	46.0%	54.0%	6.3

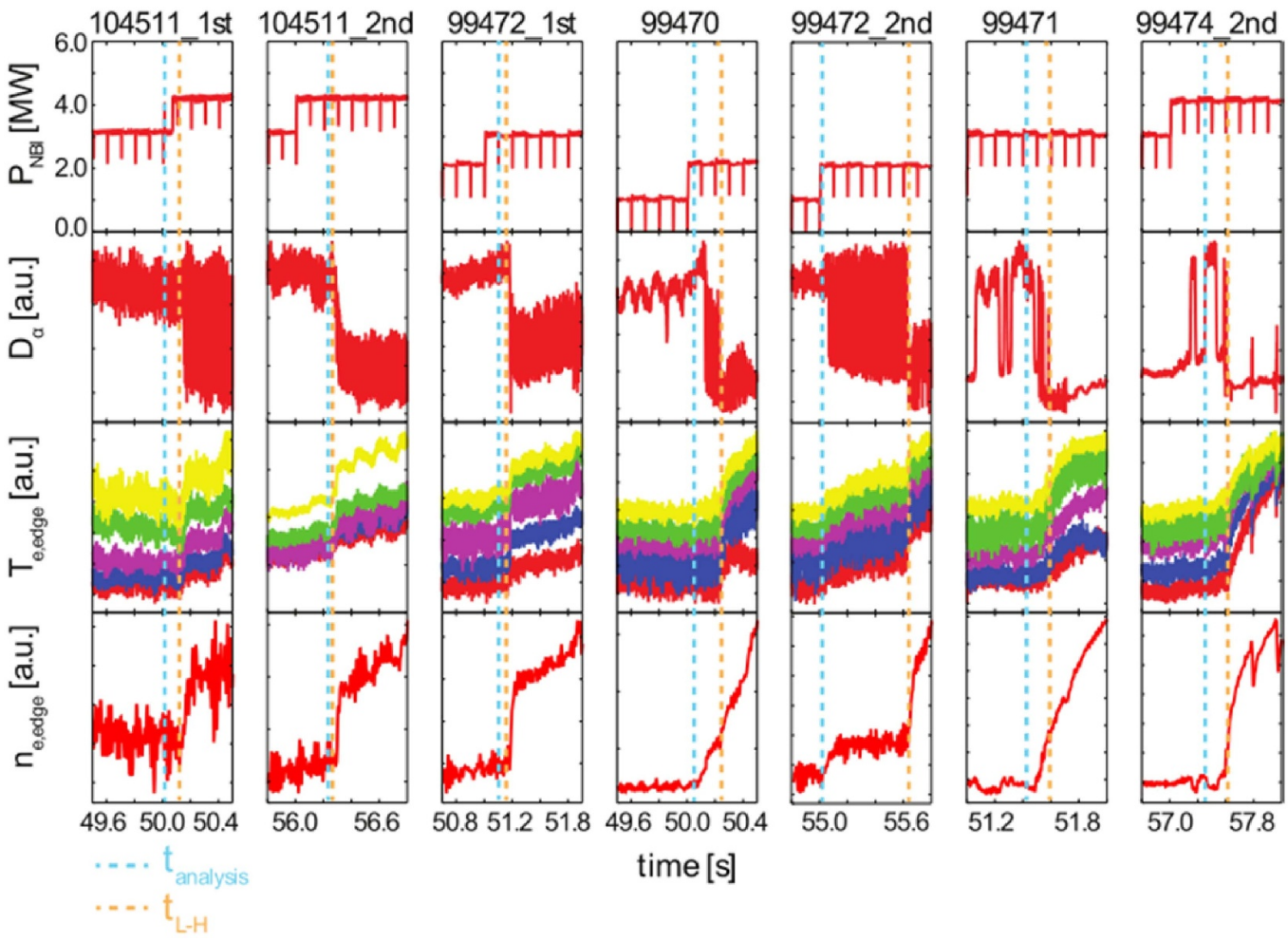


Figure 1. Identification of the L–H transition ($t_{\mathrm{L-H}}$) and analysis times (t_{analysis}) in the present dataset by (from top to bottom) NBI power, D_α emission in the divertor region, T_e from edge electron-cyclotron emission spectroscopy, and line-integrated pedestal density from interferometry in the plasma edge. In abscissa, JET machine time is represented; plasmas start at $t = 40$s.

and TC26,JET,HT (equation (3)) $P_{\mathrm{L-H}}$ scaling laws valid for the high-density branch are also plotted: the latter, JET-specific, obviously shows a better agreement to experimental points. ITPA 2008, as expected, overestimates the L–H power threshold in the high-density branch. Estimating uncertainties on P_{loss} is challenging due to NBI power modulation (see figure 1 top row) and the corresponding fast ion slowing down time compared to the modulation frequency. Since NBI is the primary source of power that triggers L–H transition, and NBI power steps are 1 MW, we decided to consider ± 0.5 MW as uncertainty. From figure 2, we clearly see the high-density branch of the transition where $P_{\mathrm{L-H}}$ increases monotonically with density, the minimum density $n_{\mathrm{e,min}}$ at $\sim 3 \cdot 10^{19}$ m^{-3} (corresponding to a Greenwald density fraction of $f_{\mathrm{GW,min}} = n_{\mathrm{e,min}}/n_{\mathrm{GW}} \sim 0.34$) and the low-density branch with the threshold power inverting the density trend. In the low-density branch, L–H transitions are often triggered by sawteeth (as 'transient L–H' transitions in figure 2). This is the case also for our lowest-density point analysed (104511, 1$^{\mathrm{st}}$ transition), characterised by a relatively large sawtooth inversion radius. These types of H-mode often barely show an improvement in confinement, which can improve later in the ramp with more power and higher density. This dynamics partly explains the scatter of $P_{\mathrm{L-H}}$ experimental points in the low-density branch, which are not well aligned and do not permit an extrapolation of $P_{\mathrm{L-H}}$ to lower densities.

Plasma kinetic profiles are a necessary ingredient for the power balance analysis since they are required for interpretative transport analysis and equipartition power calculation discussed later in section 3. Plasma electron temperature is measured with High-Resolution Thomson Scattering 'HRTS' [32, 33] and Electron Cyclotron Emission (ECE) [34] diagnostics. NBI power modulation allowed the measurement of core ion temperature by main-ion CX spectroscopy diagnostic [35]. Core T_i measurements extend up to $\rho_{\mathrm{tor}} \approx 0.85$ (being ρ_{tor} the square root of the normalised toroidal flux, $\rho_{\mathrm{tor}} = 1$ at the LCFS). Sparse edge T_i measurements by charge-exchange (CX) spectroscopy [36] are available in a few time slices and indicate that $T_i \approx T_e$ within error bars in $\rho_{\mathrm{tor}} > 0.85$. Plasma electron density is measured by HRTS and reflectometry [37, 38]. Plasma radiation losses considered for P_{sep} evaluation in the power balance analysis (section 3) are obtained by tomographic inversion of bolometry measurements [39, 40]. Similarly to [24], we have excluded edge bolometer channels

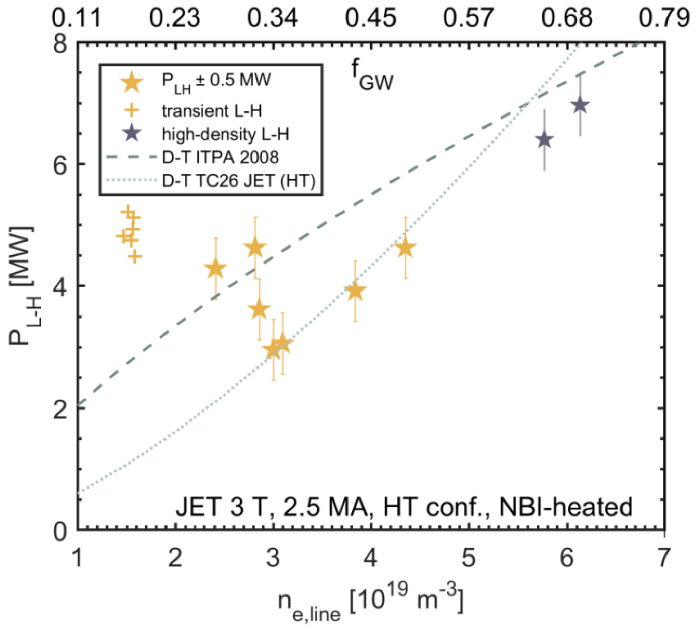


Figure 2. L–H power threshold as a function of line-averaged density for D–T plasmas. We added low-density transient L–H transitions and two high-density transitions (not analysed in the transport study below) to characterise $P_{\mathrm{L–H}}$ density branches. $P_{\mathrm{L–H}}$ scaling laws are corrected by the $\frac{2}{A_{\mathrm{eff}}}$ factor, assuming $A_{\mathrm{eff}} = 2.5$. The top x-axis represents the corresponding Greenwald density fraction.

from the radiation computation due to insufficient resolution to distinguish from the LCFS and the scrape-off layer (SOL) regions. Uncertainties on plasma radiation power are on the order of $<10\%$. In figure 3, we report plasma kinetic profiles at the analysis time selected before the L–H transition.

3. Power balance analysis to quantify the ion heat flux at the L–H transition

A power balance analysis is needed to calculate the power carried by plasma ions Q_{i} during the L–H transition (i.e. the ion heat flux) by separating all power contributions to P_{loss} (equation (1)). All terms are estimated by interpretative simulations by the JETTO transport code [41] within the JINTRAC suite of codes [42]. Fusion power is included in the power balance, though negligible since we consider L-mode plasmas, and it is here calculated with a fast analytical model for alpha particle slowing down [43] and power distribution between electrons and ions [44]. Simulations are run for 1 s before the L–H transition to consider multiple energy confinement times (typically in the order of 0.1 s), and power balance terms are then extracted at the L–H transition analysis time. NBI power coupled to plasma ions and electrons is calculated with ASCOT code [30], considering fast particle losses. Typical beam fast ion slowing down time is comparable to the plasma energy confinement time and therefore shorter than the simulation time to allow fast ion thermalisation. Plasma equilibrium used both for profile fitting and numerical simulations is obtained by pressure-constrained EFIT++ (also called 'EFTP' reconstruction) [45, 46]. Kinetic profiles obtained as described in section 2 are used as input for interpretative simulations. Figure 4 shows the result of the power balance analysis at the L–H transition for the D–T dataset. We remind that radiation power is obtained with integration up to $\rho_{\mathrm{tor}} \approx 0.95$ to exclude significant reconstruction uncertainties at the edge. Power terms evaluated from numerical simulations have been considered with an uncertainty of 10%, which is a commonly accepted error bar (similar to what was done in [8, 19]; see also discussions in [24] and [29] for NBI power uncertainties). The result of the power balance analysis is reported in figure 4(a). First, density branches are seen in both P_{loss} and P_{sep} terms. The time derivative of the energy content varies between $\sim$0.05 MW and 0.5 MW, while alpha power is negligible, below 0.03 MW. The power carried by ions (Q_{i}) also follows a similar non-monotonic trend in density, with a clear minimum at the $n_{\mathrm{e,min}}$ of this dataset. Power carried by electrons (Q_{e}) results instead almost constant, slightly decreasing throughout density branches from 2 MW to 1.5 MW. Low- and high-density transitions are characterised by $Q_{\mathrm{i}} > Q_{\mathrm{e}}$, while, at the P_{loss} minimum, $Q_{\mathrm{i}} \approx Q_{\mathrm{e}}$. At the minimum indeed, the NBI power ratio to electrons is the largest (see table 1), while absolute NBI power coupled to ions is minimum (see figure 4(b)): this is a similar trend to JET D NBI-heated dataset in [24], as discussed later in section 4. NBI ratio to electrons/ions is determined by multiple entangled effects such as plasma critical energy, strongly depending on local electron temperature, and fast ion ionisation position, depending on plasma density and injection energy.

Similarly to [24], due to the lack of consistent edge T_{i} measurements for all time slices considered in the analysis that do

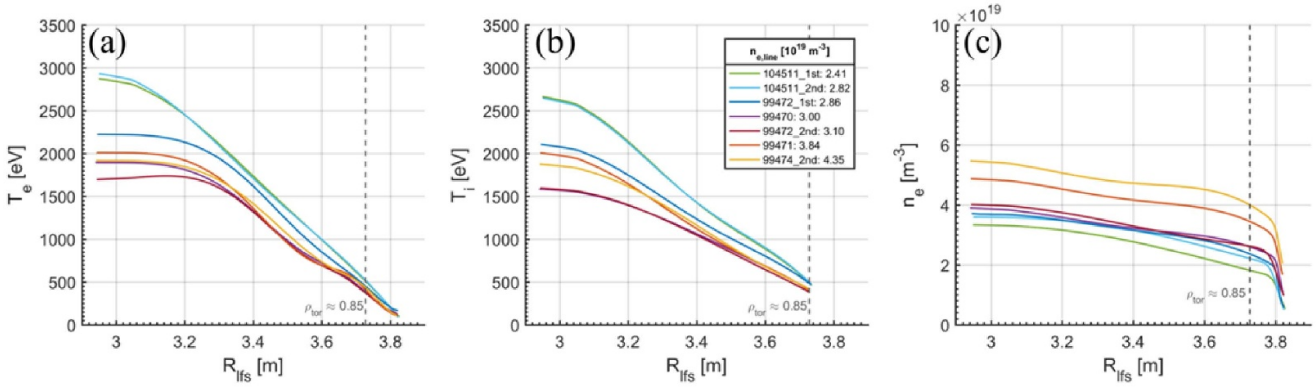


Figure 3. Plasma kinetic profiles (electron temperature in (*a*), ion temperature in (*b*), and electron density in (*c*)), before the L–H transition, obtained by fitting experimental measurements described in section 2 for the analysed D–T pulses versus the major radius in the low field side of JET R_{lfs}. We reported the approximate position of $\rho_{tor} \approx 0.85$, the boundary condition for core T_i measurement availability.

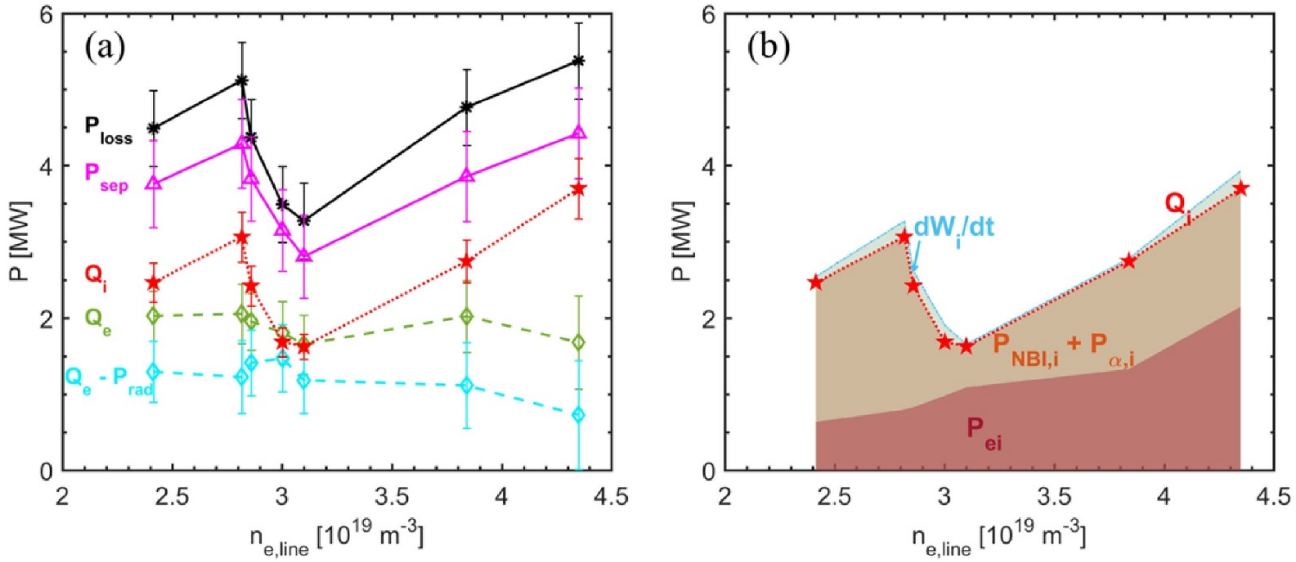


Figure 4. Results of power balance analysis with terms contributing to the power coupled to the plasma at the L–H transition ($t = t_{analysis}$) (*a*) as a function of the line-averaged electron density. (*b*) Shows the power terms contributing to the ion heat flux Q_i. Power terms are defined in equations (1), (4) and (5).

not allow to estimate ($T_e - T_i$) terms in the edge with accuracy, we decided to calculate the equipartition power P_{ei} integrating up to $\rho_{tor} = 0.85$, assuming $P_{ei} \approx 0$ (i.e. $T_e \approx T_i$) for $\rho_{tor} > 0.85$. Figure 4(*b*) shows the magnitude of terms contributing to the ion heat flux Q_i. We can observe that the equipartition power P_{ei} increases with density (as expected), and it is always in favour of ions due to $T_e > T_i$. Q_i is therefore determined mainly by NBI power at low density and equipartition power at high density, similarly to D counterpart cases [24]. We also report that from the minimum region to the high-density branch, the NBI power ratio is in favour of plasma electrons, while it is strongly in favour of plasma ions in the low-density branch (see table 1).

We have performed a specific numerical sensitivity analysis to evaluate the impact of assuming $P_{ei} \approx 0$ for $\rho_{tor} > 0.85$ (equivalent to $T_i \approx T_e$ outside $\rho_{tor} = 0.85$) on our results. We tested the sensitivity of edge P_{ei} imposing an ion temperature variation outside $\rho_{tor} = 0.85$, with $T_{i,edge} = T_{e,edge} \pm 10\%$ (typical temperature error bars in our dataset) and then integrated P_{ei} up to $\rho_{tor} = 0.95$, as done in [19] when calculating the edge ion heat flux. We also note that T_i/T_e at $\rho_{tor} \approx 0.85$ is within the range between 0.9 and 1.1 at the analysis time before the L–H transition. We finally obtain a variation of P_{ei} with respect to what was calculated for figure 4 as reported in figure 5, where the lower error bar corresponds to $T_{i,edge} > T_{e,edge}$ (negative contribution to P_{ei}) and upper error bars to $T_{i,edge} < T_{e,edge}$. The ion heat flux Q_i, also considering these P_{ei} variations, does not change its trend in density, and we can consider our results robust.

4. Investigation of ion heat flux origin and comparison to deuterium plasmas

Thanks to the experimental setup similarities to JET NBI-heated deuterium plasmas discussed in [24], we can directly

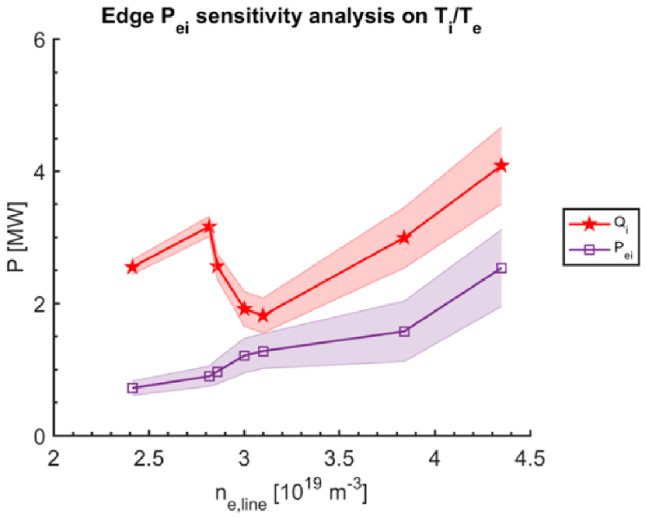


Figure 5. Sensitivity analysis on the equipartition power P_{ei} and Q_i assuming $T_i = T_e$ outside $\rho_{tor} = 0.85$ (symbols)—as done for figure 4—and variations due to $T_{i,edge} = T_{e,edge} \pm 10\%$ ($\rho_{tor} > 0.85$) in P_{ei} term, with P_{ei} integrated up to $\rho_{tor} = 0.95$.

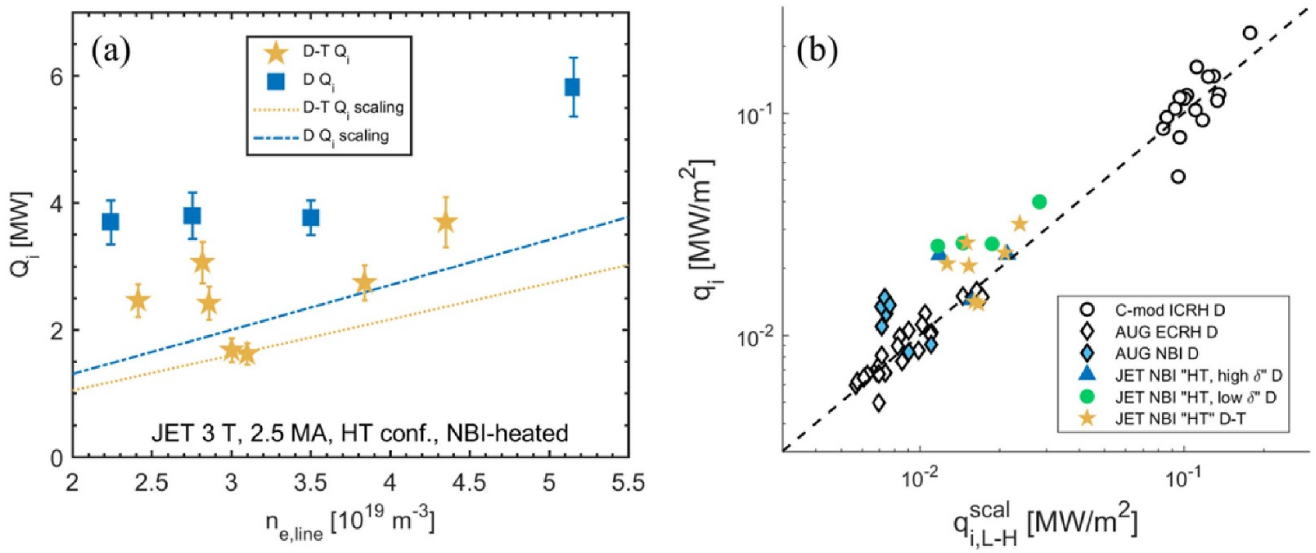


Figure 6. Comparison of the ion heat flux Q_i for the D dataset at the L–H transition of [24] and D–T dataset analysed in this paper—figure (*a*). In (*a*), Q_i scaling from equation (4) of [23] is also represented, assuming an isotope correction factor of 2/2.5 = 0.8 for the D–T dataset. Figure (*b*) shows the comparison of the ion heat flux per unit of plasma surface q_i at L–H transition (*y*-axis) versus the $q_{i,L-H}$ scaling in equation (3) of [23] (*x*-axis). Figure (*b*) includes L–H transitions of AUG and C-mod tokamaks (courtesy of J. Hughes and F. Ryter).

compare Q_i at the L–H transition in D vs D–T isotope plasmas (in figure 6(*a*)) at the samemagnetic field, plasma current, heating scheme and divertor configuration (horizontal target 'HT'). For this comparison, we select the deuterium dataset marked as 'HT, low δ' in [24] since it is the only D 'HT' dataset to have core T_i measurements. In both isotope datasets, Q_i is not monotonically increasing in density, with a deep minimum evident in the D–T dataset and a clear change of slope in D at $n_{e,min}$. We also observe that D–T Q_i is lower than D Q_i, possibly indicating some isotope effect on the ion heat flux. Looking at the high-density branch of the two datasets (D from $n_{e,line} \sim 3.5 \cdot 10^{19}$ m^{-3}, D–T from $\sim 3 \cdot 10^{19}$ m^{-3}), we can estimate a ratio between $Q_{i,D-T}$ and $Q_{i,D}$ by linear interpolation, resulting in a ratio of 0.80 ± 0.12, though based only on 2 points for D and 3 for D–T. This ratio would agree with the classical P_{L-H} isotope effect of $\frac{A_{eff,D}}{A_{eff,D-T}} = \frac{2}{2.5} = 0.8$. The extension of Q_i scaling [23], derived from wave-heated D plasmas, to other isotopes, is unknown (see e.g. the discussion in [47]). Assuming the validity of the 2/2.5 = 0.8 factor for D–T Q_i, the result of the scaling law is plotted in figure 6(*a*). Also, for the D–T dataset, Q_i scaling [23] disagrees with our experimental observation, nor is it in the high-density branch, which has a different slope in density. Looking at figure 6(*b*), we can confirm that NBI-heated plasmas, also in D–T, do not follow the wave-heated (isotope-corrected) Q_i scaling, similarly to D plasmas of JET [24] and AUG [19] NBI-heated plasmas. We also note that errors in the regression parameters of the Q_i scaling law are pretty significant ($\sim$10% on n_e, >40% on B_T, and

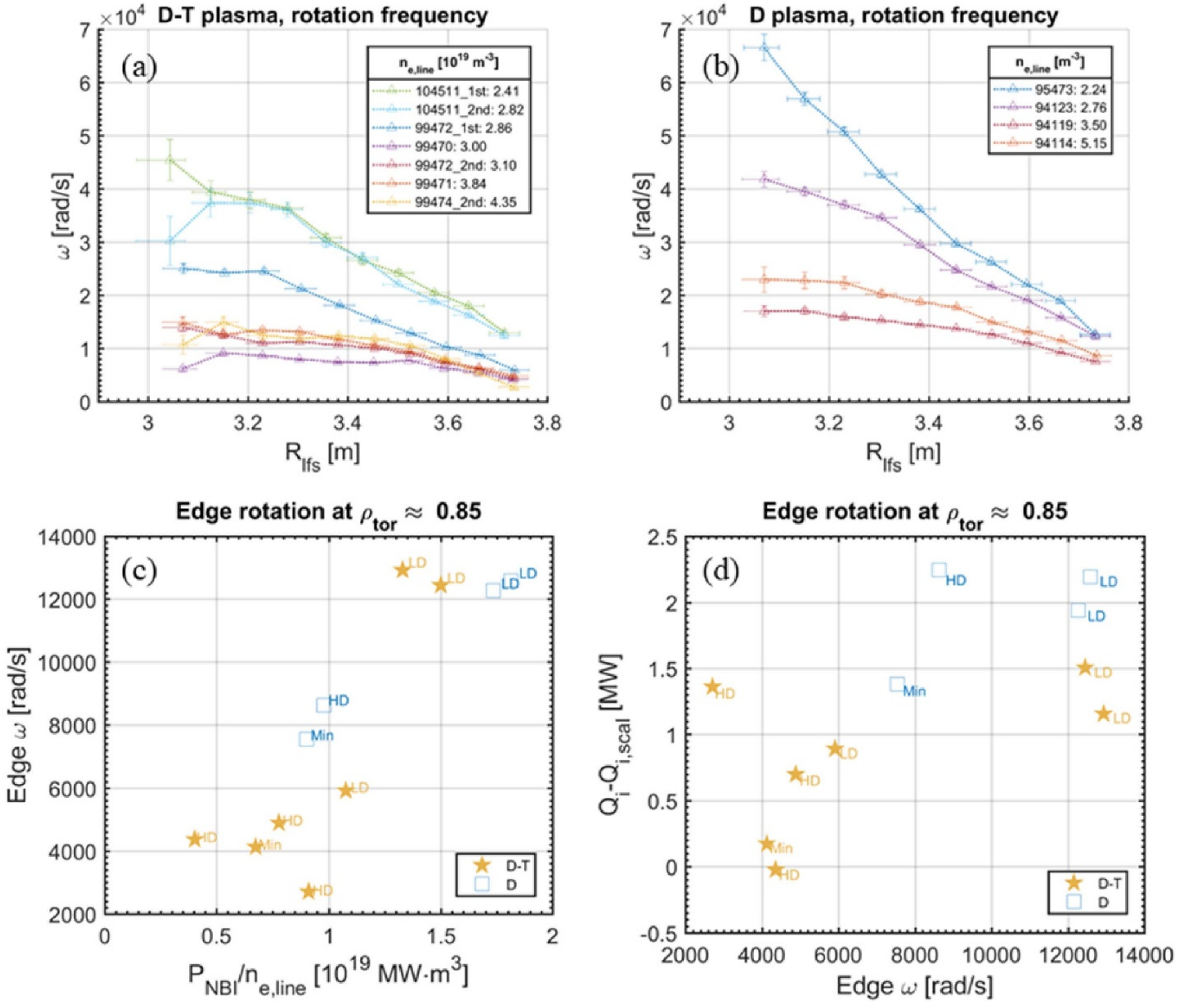


Figure 7. (*a*) Core rotation frequency profiles for D–T pulses at the L–H transition analysed in this paper. (*b*) Core rotation frequency profiles for D pulses at the L–H transition analysed in [24]. Rotation profile measurements in (*a*) and (*b*) are limited to $\rho_{tor} \approx 0.85$, similar to T_i profiles discussed in section 2. (*c*) Edge rotation frequency (i.e. at $\rho_{tor} \approx 0.85$) at the L–H transition versus the ratio of NBI power to line-averaged electron density. (*d*) Deviation of ion heat flux at the L–H transition from the Q_i scaling law in equation (4) of [23] versus edge rotation frequency. The Q_i scaling law is isotope-corrected, assuming a $\frac{2}{A_{eff}}$ factor with $A_{eff} = 2.5$ for D–T. In (*c*) and (*d*), data are labelled with the corresponding density branch of the L–H transition: 'LD' = low-density branch, 'Min' = $n_{e,min}$, 'HD' = high-density branch.

>20% on S exponents), and Q_i scaling error bars would cover almost the entire plot of figure 6(*a*).

At AUG [19], NBI-heated L–H transitions are found to deviate from Q_i scaling [23], similarly to JET (see figure 6(*b*)). This deviation and $n_{e,min}$ existence is explained at AUG with the increased plasma rotation caused by NBI, proved by L–H transitions obtained by a scan in NBI + ECRH power at the same plasma density, magnetic field, and plasma current (i.e. same power threshold from scaling laws). Evidence regarding this hypothesis at JET needs to be clarified, noting that no significant change in the shear flow has been observed preceding the L–H transition [48]. First, we are not aware of well-diagnosed D or D–T experiments where H-mode is accessed at different NBI powers at the same plasma density, e.g. by substituting part of NBI power with ICRH power (though ICRH-heated L–H transitions show at JET an increase of radiated power [4]). Some experiments with NBI + ICRH power mix were conducted in JET-ILW H plasmas but without ion heat flux information [49]. Second, in [4], it is shown that, in JET D and T plasmas at $B_T = 2.4$ T and $I_p = 2$ MA, there is not always a clear difference between P_{loss} (and P_{sep}) in NBI and ICRH-heated transitions, while no difference at all in $n_{e,min}$.

Our D–T and D datasets only have rotation profiles up to $\rho_{tor} \approx 0.85$, similar to T_i (while in [19], edge rotation is evaluated at $\rho_{tor} \approx 0.95$). Plasma rotation profiles are shown in figure 7(*a*) for D–T and (*b*) for D. We use, therefore, the outermost point for the estimation of edge rotation in our analysis. Edge rotation shows, in our case, a general increase with injected torque NBI, though with some scattering, explained by the fact that NBI power required to access H-mode (table 1) is larger both at low and high density, while plasma rotation generally decreases with plasma density. Edge rotation aligns quite well with P_{NBI}/n_e for both isotope datasets—figure 7(*c*). We also note that edge rotation does not differ significantly between D and D–T at low plasma density, while it is larger for

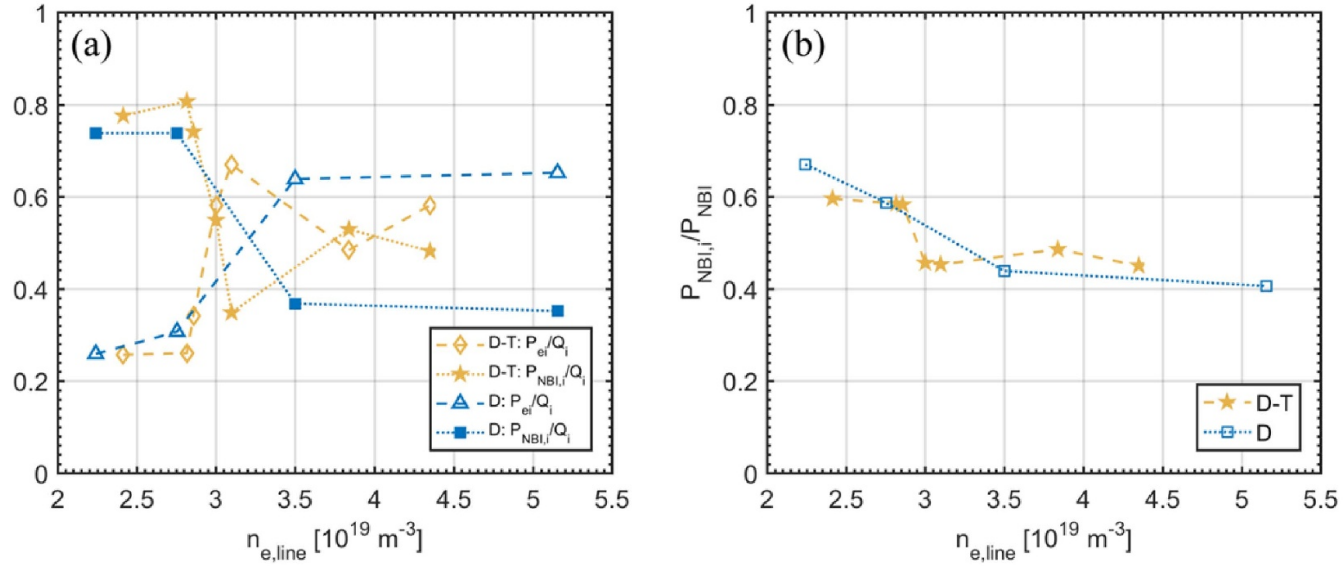


Figure 8. The ratio of equipartition power and NBI power to ions to ion heat flux Q_i at the L–H transition for D and D–T datasets (*a*). In (*b*), the NBI power ratio coupled to plasma ions is represented versus plasma density for the two datasets.

the D dataset at higher densities. As discussed previously, we noted that all P_{loss}, Q_i, P_{NBI}, and $P_{NBI,i}$ terms at the L–H transition show a minimum at $n_{e,min}$. Due to this non-monotonic behaviour of Q_i and due to edge rotation depending on n_e and P_{NBI}, we do not see a clear trend in Q_i versus edge rotation. It is more interesting to plot the deviation of Q_i at the L–H transition with respect to Q_i scaling [23]—ΔQ_i—versus the edge rotation (figure 7(*d*)). We do see a general increase of ΔQ_i with edge rotation, with a significant deviation in low-density 'LD' transitions, however, we cannot conclude that a significant deviation is (only) due to rotation. The reason is that the 'HD' point at low edge rotation shows a large ΔQ_i, similar to 'LD' points. This point is not an 'outlier' since, if we look at figure 6(*a*), we see that Q_i has a significant deviation from the scaling not only at low density but also at high density, where edge rotation is low. We expect the low-rotation high-ΔQ_i area to be even more populated with more Q_i points from high-density transitions. With a Q_i scaling law that better fits the high-density branch Q_i points at JET, we would probably exclude low-rotation high-ΔQ_i points and see a correlation between ΔQ_i and edge rotation density in the low-density branch. Unfortunately, we do not have sufficient data to generate a JET Q_i scaling law for the high-density branch of the transition. In conclusion, low-density branch Q_i points may deviate from density linearity due to edge rotation. Still, we note an unsatisfactory agreement of Q_i scaling also in the high-density branch at low-rotation.

We now analyse what generates Q_i in D and D–T to see if there are common patterns, especially in the low-density branch where data deviate from density linearity. Figure 8(*a*) represents the relative contribution of the equipartition power and NBI power coupled to the ions to the total ion heat flux Q_i. At low density, both datasets are characterised by similar ratios of P_{ei}/Q_i and $P_{NBI,i}/Q_i$, with the contribution from NBI dominant. Please note that $P_{ei} + P_{NBI,i}$ is slightly larger than Q_i due to the presence of—$dW_{th,i}/dt$ term in Q_i. Going to high density, we observe an increase in the equipartition power P_{ei} contribution with respect to $P_{NBI,i}$ contribution. In both datasets, Q_i is therefore determined predominantly by NBI power at low density. In contrast, the relative contribution of equipartition power becomes larger at higher density and, in some cases, significantly exceeds the NBI contribution, with a slight displacement of the density at which the relative contribution change occurs. The NBI power ratio coupled to plasma ions at the L–H transition has a very similar dependence in density for D and D–T (figure 8(*b*)). Both equipartition and NBI power ratio to ions strongly depend on kinetic plasma profiles. Beam injection energy is similar in the datasets, with the only difference that in most of the D–T dataset, NBI also injects tritium, with a deuterium to tritium injection velocity ratio proportional to $\frac{v_D}{v_T} \propto \sqrt{\frac{m_T}{m_D}} \cong 1.2$, which does not significantly change the beam absorption. The similar behaviour we note for P_{ei} and $P_{NBI,i}$ relative contributions to Q_i might be explained by similar kinetic properties of the plasmas at the same plasma density, independently from the isotope. Indeed, in JET experiments, electron temperature profiles measured at the L–H transition show similarities independently from the hydrogenic plasma effective mass [6].

5. Conclusion

Understanding the physics governing the L–H transition is crucial to predicting performance and designing next-step fusion devices. Entering the H-mode close to the minimum density $n_{e,min}$ would permit the reduction of the requested amount of power to be coupled to the plasma. The origin of $n_{e,min}$ is still unclear, and it may be linked to the critical power coupled to plasma ions Q_i that is required to enter the H-mode, as hypothesised in [19]. NBI-heated plasmas at JET

are seen to deviate from the Q_i scaling law obtained in wave-heated D plasmas [23], which foresees a linear dependence of Q_i on plasma density. In the present paper, we characterised D–T L–H transitions from low- to high-density branches, directly comparing them with similar experiments in D [24]. Regrettably, these NBI-heated D–T L–H transition experiments could be the last of this kind before ITER nuclear phase operations. Our D–T dataset clearly shows a minimum in the L–H power threshold, at $n_{e,min} \approx 3 \cdot 10^{19}$ m^{-3}. Through interpretative transport modelling, we evaluated the power carried by plasma ions Q_i at the transition (i.e. the ion heat flux). Q_i shows a clear minimum at $n_{e,min}$, like the power threshold. This finding is similar to NBI-heated JET D plasmas, showing a deviation from wave-heated Q_i scaling proposed in [20]. The extension of this scaling to D–T plasmas is unknown, and we applied the classical $\frac{A_{eff,D}}{A_{eff,D-T}} = \frac{2}{2.5} = 0.8$ factor for $\frac{Q_{i,D-T}}{Q_{i,D}}$, which seems to agree when comparing JET observed D and D–T Q_i. In AUG NBI-heated L–H transitions [19], deviation from Q_i scaling is explained by edge plasma rotation induced by NBI. Though we could not replicate the same mixed NBI/wave heating experiments at JET, we compared the deviation from Q_i scaling to the edge plasma rotations in our D and D–T datasets. We see a significant deviation from the scaling both at low edge rotation (high-density branch of the transition) and high edge rotation (low-density branch). We note that Q_i scaling does not fit well Q_i either in the high-density branch. With a better fitting of JET NBI-heated high-density Q_i points, the deviation from a quasi-linear density scaling could be correlated with high edge rotation at low density. This hypothesis, however, would need further experiments and analysis.

We finally see a common origin of the ion heat flux in D and D–T NBI heated L–H transitions: at low density, Q_i is dominated by NBI power, while, at high density, equipartition power contribution becomes larger, approaching and, in some cases, significantly exceeding the NBI power coupled to plasma ions.

To summarise, we leave some open questions on what generates the minimum density in JET plasmas, but we have findings that the ion heat flux Q_i in NBI-heated L–H transitions deviates from linearity in density in the low-density branch, with common features between D and D–T datasets. We also see an isotope effect on Q_i. Edge rotation can play a role, although a direct comparison of Q_i in NBI and wave-heated plasmas at JET has not been possible.

Acknowledgment

This work has been carried out within the framework of the EUROfusion Consortium, funded by the European Union via the Euratom Research and Training Programme (Grant Agreement No 101052200—EUROfusion). Views and opinions expressed are however those of the author(s) only and do not necessarily reflect those of the European Union or the European Commission. Neither the European Union nor the European Commission can be held responsible for them. This research was supported in part by the Grants FIS2017-85252-R and PID2021-127727OB-I00, funded by the Spanish MCIN/AEI/ 10.13039/501100011033 and by "ERDF A way of making Europe. Work supported, in part, by the US DOE under Contract No. DE-AC05-00OR22725 with UT-Battelle, LLC. J. Hughes and F. Ryter have kindly provided Alcator C-mod and ASDEX-Upgrade data for figure 6. Last, as the first author, I would like to acknowledge the whole 'JET L–H transition' team as mentioned in [4].

ORCID iDs

P. Vincenzi https://orcid.org/0000-0002-5156-4354
E.R. Solano https://orcid.org/0000-0002-4815-3407
E. Delabie https://orcid.org/0000-0001-9834-874X
C. Angioni https://orcid.org/0000-0003-0270-9630
G. Birkenmeier https://orcid.org/0000-0001-7508-3646
C. Maggi https://orcid.org/0000-0001-7208-2613
R.B. Morales https://orcid.org/0000-0003-0667-3356
H.J. Sun https://orcid.org/0000-0003-0880-0013
E. Tholerus https://orcid.org/0000-0002-3262-1958

References

[1] Shimada M. *et al* 2007 Progress in the ITER physics basis chapter 1: overview and summary *Nucl. Fusion* **47** S1
[2] Martin Y. *et al* 2008 *J. Phys.: Conf. Ser.* **123** 012033
[3] Wenninger R. *et al* 2017 *Nucl. Fusion* **57** 016011
[4] Solano E.R. *et al* 2023 *Nucl. Fusion* **63** 112011
[5] Righi E. *et al* 1999 *Nucl. Fusion* **39** 309
[6] Birkenmeier G. *et al* 2023 *Plasma Phys. Control. Fusion* **65** 054001
[7] Maggi C. *et al* 2014 *Nucl. Fusion* **54** 023007
[8] Ryter F. *et al* 2013 *Nucl. Fusion* **53** 113003
[9] Delabie E. *et al* 2017 Status of TC-26: L-H/H-L scaling in the presence of metallic walls *ITPA Meeting, Private Communication* (*St. Paul-lez-Durance, France, 17–20 September 2018*)
[10] Solano E.R. *et al* 2022 *Nucl. Fusion* **62** 076026
[11] Fielding S.J., Valovic M., Carolan P.G., Gates D.A., Hunt C., Leahy P. and Morris A.W. (the COMPASS-D Physics and ECRH Teams) 1998 *Plasma Phys. Control. Fusion* **40** 731
[12] Ryter F. *et al* 2009 *Nucl. Fusion* **49** 062003
[13] Gohil P., Evans T.E., Fenstermacher M.E., Ferron J.R., Osborne T.H., Park J.M., Schmitz O., Scoville J.T. and Unterberg E.A. 2011 *Nucl. Fusion* **51** 103020
[14] Ma Y., Hughes J.W., Hubbard A.E., LaBombard B., Churchill R.M., Golfinopolous T., Tsujii N. and Marmar E.S. 2012 *Nucl. Fusion* **52** 023010
[15] Horton L.D. *et al* 1999 Dependence of the H-mode threshold on the JET divertor geometry (ECA) vol 23J p 193
[16] Righi E., Campbell D.J., Conway G.D., Hawkes N.C., Horton L.D., Maggi C.F., Saibene G., Sartori R. and Zastrow K.-D. 2000 *Plasma Phys. Control. Fusion* **42** A199–A204
[17] Sartori R. *et al* 2004 *Plasma Phys. Control. Fusion* **46** 723–50
[18] Andrew Y. *et al* 2006 *Plasma Phys. Control. Fusion* **48** 479
[19] Ryter F., Barrera Orte L., Kurzan B., McDermott R.M., Tardini G., Viezzer E., Bernert M. and Fischer R. 2014 *Nucl. Fusion* **54** 083003
[20] Maggi C.F. *et al* 2018 *Plasma Phys. Control. Fusion* **60** 014045
[21] Sauter P., Pütterich T., Ryter F., Viezzer E., Wolfrum E., Conway G.D., Fischer R., Kurzan B., McDermott R.M. and Rathgeber S.K. 2012 *Nucl. Fusion* **52** 012001
[22] Ryter F. *et al* 2016 *Plasma Phys. Control. Fusion* **58** 014007

[23] Schmidtmayr M. *et al* 2018 *Nucl. Fusion* **58** 056003
[24] Vincenzi P. *et al* 2022 *Plasma Phys. Control. Fusion* **64** 124004
[25] Maggi C.F. *et al* 2024 *Nucl. Fusion* **64** 112012
[26] Meister H. *et al* 2004 *Rev. Sci. Instrum.* **75** 4097–9
[27] Neverov V.S., Kukushkin A.B., Kruezi U., Stamp M.F. and Weisen H. 2019 *Nucl. Fusion* **59** 046011
[28] Vartanian S. *et al* 2021 *Fusion Eng. Des.* **170** 112511
[29] King D.B. *et al* 2023 *Nucl. Fusion* **63** 112005
[30] Hirvijoki E., Asunta O., Koskela T., Kurki-Suonio T., Miettunen J., Sipilä S., Snicker A. and Äkäslompolo S. 2014 *Comput. Phys. Commun.* **185** 1310–21
[31] Solano E.R. *et al* 2017 *Nucl. Fusion* **57** 022021
[32] Pasqualotto R., Nielsen P., Gowers C., Beurskens M., Kempenaars M., Carlstrom T. and Johnson D. 2004 *Rev. Sci. Instrum.* **75** 3891
[33] Frassinetti L., Beurskens M.N.A., Scannell R., Osborne T.H., Flanagan J., Kempenaars M., Maslov M., Pasqualotto R. and Walsh M. 2012 *Rev. Sci. Instrum.* **83** 013506
[34] de la Luna E., Sánchez J., Tribaldos V., contributors J.-E., Conway G., Suttrop W., Fessey J., Prentice R., Gowers C. and Chareau J.M. 2004 *Rev. Sci. Instrum.* **75** 3831–3
[35] Hawkes N.C., Delabie E., Menmuir S., Giroud C., Meigs A.G., Conway N.J., Biewer T.M. and Hillis D.L. 2018 *Rev. Sci. Instrum.* **89** 10D113
[36] Delabie E., Hawkes N., Biewer T.M. and O'Mullane M.G. 2016 *Rev. Sci. Instrum.* **87** 11E525
[37] Sirinelli A. *et al* 2010 *Rev. Sci. Instrum.* **81** 10D939
[38] Morales R.B. *et al* 2024 *Rev. Sci. Instrum.* **95** 043501
[39] Ingesson L.C. *et al* 1997 *Part I Proc. 24th EPS Conf. on Controlled Fusion and Plasma Physics* (*Berchtesgaden, Germany*, *9–3 June 1997*) vol 21A (EPS) pp 113–6
[40] Ingesson L.C., Alper B., Chen H., Edwards A.W., Fehmers G.C., Fuchs J.C., Giannella R., Gill R.D., Lauro-Taroni L. and Romanelli M. 1998 *Nucl. Fusion* **38** 1675
[41] Cenacchi G. and Taroni A. 1988 *Rapporto ENEA RT/TIB*(88)5
[42] Romanelli M. *et al* 2014 *Plasma Fusion Res.* **9** 3403023
[43] Estrada-Mila C., Candy J. and Waltz R.E. 2006 *Phys. Plasmas* **13** 112303
[44] Mikkelsen D.R. and Singer C.E. 1983 Optimization of steady-state beam-driven tokamak reactors *Nucl. Technol. Fusion* **4** 237–52
[45] Brix M., Hawkes N.C., Boboc A., Drozdov V. and Sharapov S.E. 2008 *Rev. Sci. Instrum.* **79** 10F325
[46] Szepesi G. *et al* 2021 Advanced equilibrium reconstruction for JET with EFIT++ *47th EPS Conf.* (*21–25 June 2021*) P3.1037 (available at: https://info.fusion.ciemat.es/OCS/eps2021pap/pdf/P3.1037.pdf)
[47] Angioni C., Citrin J., Loarte A., Polevoi A.R., Kim S.H., Fable E. and Tardini G. 2023 *Nucl. Fusion* **63** 126035
[48] Silva C., Solano E.R., Hillesheim J.C., Delabie E., Birkenmeier G., Gil L., Giroud C., Morales R.B. and Nina D. 2022 *Nucl. Fusion* **62** 126057
[49] Hillesheim J. *et al* 2017 L-H transition studies in hydrogen and mixed ion species plasmas in JET *44th EPS Conf. Plasma Physics P5.162* (*Belfast, Northern Ireland, UK*, *26–30 June 2017*) (available at: http://ocs.ciemat.es/EPS2017PAP/pdf/P5.162.pdf)